Published in final edited form as:
Neuroimage. 2010 April 1; 50(2): 465–471. doi:10.1016/j.neuroimage.2009.12.057.

Microscopic Diffusion Tensor Imaging of the Mouse Brain

Yi Jiang and **G. Allan Johnson**
Center for In Vivo Microscopy, Box 3302, Duke University Medical Center, Durham, NC 27710, USA

Abstract

Diffusion tensor imaging (DTI) data at 43 μm isotropic resolution has been acquired on the intact adult mouse brain in 28-hour scan time by using a streamlined protocol, including specimen fixation and staining, image acquisition, reconstruction, post-processing, and distribution. An intermediate registration of each component image is required to achieve the desired microscopic resolution. Multiple parameters have been derived, including fractional anisotropy, axial and radial diffusivity, and a color-coded orientation map of the primary eigenvector. Each DTI dataset was mapped to a common reference space to facilitate future standardized analysis. Fiber tracking has also been demonstrated, providing 3D connection information. This protocol to acquire high-resolution DTI data in a robust and repeatable fashion will serve as a foundation to quantitatively study mouse brain integrity and white matter architecture, at what we believe to be the highest spatial resolution yet attained.

INTRODUCTION

Advances in molecular biology have provided unprecedented opportunities to use versatile small animal platforms (most importantly, the mouse) for connecting genotypes and phenotypes of brain development, damage, or repair associated with specific pathologies (Badea et al., 2009; Chesler et al., 2003). Diffusion tensor imaging (DTI) (Basser et al., 1994) of the mouse brain has resulted in extraordinary new insight into the brain structure, connectivity, and integrity in normal and diseased brains, especially in white matter regions (Mori et al., 2001; Song et al., 2005). DTI provides a unique composite contrast reflecting tissue diffusivity, anisotropy, and directionality, which can also be used to track fibers (Mori et al., 1999) to yield detailed three-dimensional connectivity information, offering a complementary alternative to the traditional histological methods.

Due to the nature of signal attenuation in diffusion-weighted imaging and the requirement of multiple images with different diffusion weighting gradients, DTI requires a much longer scan time than conventional magnetic resonance imaging (MRI) to acquire a complete dataset with sufficient signal-to-noise-ratio (SNR). The scan time/SNR constraint is more prominent for high-resolution DTI, which is essential to image a small specimen such as the mouse brain. Current state-of-the-art DTI methods enable imaging an ex vivo adult mouse brain at approximately 120 μm isotropic resolution (1700 pl voxel) within approximately one day of scan time (Verma et al., 2005; Zhang et al., 2005). Since DTI models all the tissues inside one voxel as a single ellipsoid, it is of great benefit to acquire higher-resolution data, i.e. smaller

Correspondence: G. Allan Johnson Center for In Vivo Microscopy Box 3302, Duke University Medical Center Durham, NC 27710, USA Phone: 919 684-7754 Fax: 919 684-7158 gjohnson@duke.edu.

voxels to reduce partial volume effects, resolve finer structures, and improve fiber tracking accuracy. Two technical issues make microscopic DTI challenging—the signal from the small voxels is very weak and the data arrays are exceptionally large.

In this study, streamlined methods for specimen fixation and staining, image acquisition, reconstruction, post-processing, and distribution have been devised to form an efficient protocol to obtain DTI datasets at 43 μm isotropic resolution with SNR • 50 for the non-diffusion-weighted (b0) image, and SNR • 30 for the diffusion-weighted image (DWI) within 28 hours scan time. The spatial resolution (80 pl voxel) allowed DTI parameters to be quantitatively measured at approximately 7 million locations throughout the mouse brain. The DTI dataset of each individual brain is mapped to a common reference space defined by a collection of very high-resolution (21.5 μm) MR images with matching Nissl sections. This standardized coordinate system has been developed by the Digital Atlasing Task Force of the International Neuroinformatics Coordinating Facility <www.incf.org>. The coordinate system, called "Waxholm Space" (WHS) in reference to the Swedish city where this committee first met, has been developed to allow scientists to share many different types of data in a common reference space. The DTI data is now part of the Biomedical Informatics Research Network (BIRN) network (Johnson et al., 2007), which enables investigators from any place on the globe to access quantitative mouse brain anatomy in a routine and standardized fashion. All of the data in this study is available at <www.civm.duhs.duke.edu/neuro200902/index.html>.

MATERIALS AND METHODS

Fig. 1 provides a schematic of the workflow and integration of the methods discussed in this paper. All animal studies were performed under protocols approved by the Duke Institutional Animal Care and Use Committee. The images presented here are of adult (9–12 weeks) male C57BL/6 mice (Charles River, Raleigh, NC).

Specimen Fixation and Staining

Active staining (Johnson et al., 2002) uses a contrast agent mixed with a fixative to enhance MR signal by preferentially reducing the spin lattice relaxation time (T1), while simultaneously preserving the tissue, so that conventional histology can be performed later. For this study, the method of choice for the mouse brain used a series of perfusing solutions administered via a transcardial approach. Animals were anesthetized with Nembutal. A catheter was inserted into the left ventricle of the mouse heart. The animal was perfused with a peristaltic pump, first with a mixture of 0.9% saline and ProHance® (10:1, v:v) (gadoteridol, Bracco Diagnostics, Inc., Princeton, NJ), then followed by a mixture of 10% buffered formalin and ProHance (10:1, v:v). During the entire procedure, the mouse brain remained in the cranium to avoid damage to the brain and to limit physical distortions that are inevitable when the brain is extracted from the cranium.

Image Acquisition

All images were acquired using a 9.4 T vertical bore Oxford magnet with shielded coils providing gradients of up to 2000 mT/m (Resonance Research, Inc. Billerica, MA), controlled by a GE EXCITE MR imaging console (GE Healthcare, Milwaukee, WI). An additional stage in the transceiver chain converted the transmit and receive signals via a mixer driven with an external 400-MHz oscillator. Specimens were imaged in solenoid radiofrequency coil that was built in-house, constructed from a single sheet of microwave substrate. A diffusion-weighted spin-echo pulse sequence was used to acquire 3D volume images (field of view=22×11×11 mm, matrix size=512×256×256 resulting in 43 μm isotropic resolution, TR=100 ms, TE=11.8 ms, NEX=2). Diffusion encoding was performed using a pair of half-sine gradient pulses (pulse

width=1.3 ms, pulse separation=6.4 ms, gradient amplitude=1600 mT/m). One b0 (i.e., b≈0) and 6 diffusion-weighted images (b≈1.5×10^3 s/mm^2) sensitized in 6 directions ([1, 1, 0], [1, 0, 1], [0, 1, 1], [–1, 1, 0], [1, 0, –1], [0, –1, 1]) were acquired over approximately 28 hours. T1 and T2* anatomical images with the same field of view (FOV) and resolution were also acquired with 1-hour scan time (TR=50 ms, NEX=1).

The 16-bit dynamic range of the digitizers on MR imaging systems is not adequate for image arrays much larger than 256^3 (Maudsley, 1988). A novel acquisition strategy that amplified the high-frequency information by selectively altering the receiver gain during the phase-encoding steps was applied to extend the dynamic range of the system (called “extended dynamic range”) (Johnson et al., 2007). The more peripheral parts of Fourier space were acquired with the receiver gain set as high as necessary to fill at least 15 bits of the digitizer. Towards the center of k-space, to avoid saturation of the digitizer, the analog gain was decreased in 6-dB steps. For each 6-dB step, the data sampling was doubled, which not only matched the signal level to the signal levels of the more peripheral parts of Fourier space, but also increased the dynamic range towards the center. Six gain steps were used in this experiment, with each step tailored to the magnitude of the signal in that region of Fourier space. Separate experiments have been performed previously to verify that the changes in receiver gain do not produce phase discontinuities where the receiver gain is changed. The extended dynamic range method is not sequence or scanner-dependent and can therefore be readily applied in other scenarios.

Image Reconstruction, Post-processing, and Archiving

The total size of raw data files for a DTI experiment was 1.9 GB (7×512×256×256 points with real and imaginary parts, represented as 4 bits float numbers). The reconstruction process involved a number of complex steps, each reading and writing multiple very large files. The entire process has been automated on dedicated 64-bit Silicon Graphics (Origin 3000) (Silicon Graphics International, Fremont, CA) processor with high internal bandwidth, allowing routine reconstruction and proper scaling of the DTI dataset in < 2 hours, generating a total of 500 MB of reconstructed images (one b0 and six DWIs). The T1- and T2*-weighted contrast produced an additional 537 MB of raw data, and 134 MB of image data for each brain.

To remove misregistration due to residual eddy-current induced image distortion, all DWI, T1-weighted, and T2*-weighted images were co-registered to the corresponding b0 image using a mutual information based shift-only registration program (Mistry and Hsu, 2006), which was performed in 64-bit MATLAB (The MathWorks, Natick, MA) with Fourier transform-based deformations to minimize blurring effect arising from interpolation. Because the transformation was shift only, diffusion encoding orientations did not need to be adjusted in the subsequent step of diffusion tensor computation, which was executed with multivariate linear fitting in 64-bit DTIStudio (H. Jiang and S. Mori, Johns Hopkins University, Kennedy Krieger Institute).

A brain mask was obtained for each individual brain by stripping the skull in the T1 image using an algorithm based on thresholding, mathematical morphology, and connected component analysis (Badea et al., 2007). This mask was then applied to the T2* and DTI images of the same brain. The Waxholm Space (WHS) reference space consists of 4 carefully aligned datasets of the adult C57BL/6 brain: MR histology images with T1-, T2-, and T2*-weighting have been acquired at 21.5 μm resolution without moving the specimen. The same brain was removed from the skull and serially sectioned at 20 μm, stained with Nissl, and aligned to the MR data. The T1 and T2 data have been used to perform an initial auto-segmentation of 40 structures. The boundaries of these structures have been further “tuned” by careful manual correction (Johnson et al., 2007). Finally, the T1 and T2* images of the reference brain were stripped using the same skull stripping method as the DTI data.

The T1 and T2* images after skull-stripping were used to drive the normalization process to register each individual brain to the reference brain, which was performed in 64-bit Landmarker (X. Li, H. Jiang, and S. Mori, Johns Hopkins University), using a series of registration steps in the order of rigid transformation, 12-mode linear affine transformation with Automated Image Registration (AIR) (Woods et al., 1998), and two-channel (T1 and T2* images). Large Deformation Diffeomorphic Metric Mapping (LDDMM) (Miller et al., 2005). The overall transformation matrix was then applied to the calculated diffusion tensor field to properly map and reorient the diffusion tensors (Alexander et al., 2001; Xu et al., 2003). As shown in other sections of this manuscript, the alignment of the fiber tracts derived from the DTI data with segmented structures in the WHS space provides visual feedback on the quality of the spatial normalization of the DTI data into the reference space.

The transformed diffusion tensors were diagonalized into three eigenvalues and three eigenvectors. Then, the anisotropy indices, such as the fractional anisotropy (FA) (Pierpaoli and Basser, 1996) and other derived parameters, such as the radial diffusivity (RD) (Song et al., 2005), were calculated in DTIStudio. The primary eigenvector corresponding to the largest eigenvalue was taken as representing the local fiber orientation. A 24-bit, color-coded orientation map was created by assigning red, green, and blue channels to the rostral-caudal, left-right, and dorsal-ventral components of the primary eigenvector, where intensity was proportional to FA. Fiber tracking was also performed in DTIStudio with the Fiber Assignment by Continuous Tracking (FACT) method and brute-force fiber searching approach (Mori et al., 1999; Xue et al., 1999). The fiber tracking parameters were: FA threshold for starting tracking=0.6, FA threshold for ending tracking=0.3, and fiber turning angle for ending tracking=60°. 3D image and fiber visualization was performed either in DTIStudio or Amira (Visage Imaging, San Diego, CA).

Each DTI dataset resulted in an aggregate of more than 4 GB data, including the initial b0 and DWI images, and derived data such as the diffusion tensors, eigenvalues, eigenvectors, anisotropy indices, and fiber tracts. All the related images of the same brain were added into the archive and linked to the original animal metadata via an Oracle database, which can be accessed via the Internet (Johnson et al., 2007).

RESULTS

Fig. 2 illustrates the original b0 (a) and six DWI (b-g) images of a mouse brain after skull-stripping, displayed on a horizontal plane. The intensity of each DWI image was scaled up three times to allow better visual appreciation of diffusion contrasts. The intensity asymmetry resulting from different diffusion weighting orientations is clearly presented, such as the corpus callosum shown in Fig.2b (gradient direction [1, 1, 0]) or in Fig. 2e (gradient direction [–1, 1, 0]). SNR was approximately 50 for the b0 and approximately 30 for the DWIs in these high-resolution images, where SNR was calculated as the averaged intensity in the brain region divided by the standard deviation in the background.

Fig. 3 shows two orthogonal planes of the FA map of a mouse brain before (top row) and after (bottom row) the intra-dataset registration, where each DWI was registered to the corresponding b0 image. There are discernible artifacts before the intra-dataset registration in the top row, which can be better examined in the magnified views on the right. For instance, as pointed by arrows #1, #4, and #5, false enhanced edges are formed by image misalignment; as pointed out by arrows #2 and #3, blurring and distortion of fine structures are clearly present. A number of such examples can be found by carefully examining the 3D images. Therefore, intra-dataset registration is a critical step in order to realize the high resolution inherent in the large image arrays.

Fig. 4 shows the T1-weighted image of the reference mouse brain in WHS (top row) and T1-weighted image of an individual brain in this study before (middle row) and after (bottom row) registering to the reference brain. Despite slight contrast differences between the reference brain and the individual brain, excellent image alignment resulted from the inter-dataset registration and exceptional preservation of high resolution and anatomical details can be observed by visual inspection.

The richness of the tensor information supports a number of different diffusion-related contrasts. Fig. 5 illustrates a few important contrasts derived from the diffusion tensor. FA is the fractional anisotropy, which reflects how anisotropic the diffusion in one voxel is. AD (axial diffusivity) is the primary eigenvalue, representing diffusivity along the major axis of the tissue. RD (radial diffusivity) is the mean of the secondary and tertiary eigenvalues, characterizing diffusivity perpendicular to the long axis of the tissue. Each image demonstrates a unique contrast that reveals certain aspect of the diffusion property of the underlying tissue, complementing conventional MR contrasts such as T1, T2, and T2*. For example, overall the white matter exhibits higher FA, higher AD, and lower RD than the gray matter, which is as expected, since in the axon and its surrounding extracellular space, the parallel diffusivity is higher and the perpendicular diffusivity is lower compared to the same values in the neuron soma, indicating higher anisotropy in the white matter.

Fig. 5 also shows a color-coded orientation map (the Clr panel) that more effectively presents the directional information embedded in the primary eigenvector, i.e., the local fiber orientation (Green: left-to-right; Red: rostral-to-caudal; Blue: dorsal-to-ventral). This composite color contrast incorporates information from all the original images, offering novel orientation information at very high resolution. In addition, the edges of a number of structures that are difficult to distinguish in all the other images (e.g. b0, DWI, diffusivity, or anisotropy) are well differentiated in this color display. Several examples are shown in the magnified views on the right, comparing the color representation to the FA images. In panel a, arrow #1 points to habenular commissure, providing the direction of this thin white matter bundle (generally left to right), which is very difficult to visualize at lower resolution. In panel b, fimbria (arrow #2), optic tract (arrow #3), cerebral peduncle (arrow #4), a thin branch of the optic tract (arrow #5), and a thin branch of fimbria (arrow #6) can be readily differentiated on the colormap, which is almost impossible to see in any other image. Although the cingulum appears parallel to corpus callosum in the sagittal view, panel c reveals the fiber orientation of cingulum (arrow #7), as running largely rostral to caudal (red), is almost perpendicular to the main direction of corpus callosum (arrow #8), which runs from medial to lateral (green). These examples illustrate the capability and advantage of the DTI data in this study—presenting valuable directional information at very high resolution.

Fig. 6 shows the 3D reconstruction of some exemplary fiber tracts obtained from an individual brain overlaid with a few anatomical regions labeled in the reference brain. The displayed white matter structures include: corpus callosum (red), cingulum (cyan), anterior commissure (blue), fimbria (white), optic tract (green), and habenular commissure (pink). The displayed anatomical regions in transparent color include: olfactory bulbs (light blue), anterior commissure (purple), fimbria (green), hippocampus (yellow), septal nuclei (brown), and cerebral cortex (dark blue). Fig. 6a and 6b illustrate a side view and a bottom (ventral) view (rostral on left and caudal on right) of the overall reconstruction to demonstrate the 3D spatial relationship and connection between these structures. The correspondence between the white matter fibers obtained from the individual brain and the anatomical regions defined in the reference brain confirms the quality of image registration and tensor transformation, supporting the utility of studying different brains in one common spatial coordinate system.

Due to the limitation of 2D display, structures appear overlapped with each other. Therefore, several representative structures are displayed individually to provide clearer visual examination in panels c, d, and e. Panel c shows the anterior commissure, where the anterior limbs extending to the olfactory bulbs, the posterior limbs connecting to the cerebral cortex, and the crossing of the fibers are clearly delineated. The tracked fibers match with the anterior commissure region (purple) almost perfectly. In panel d, corpus callosum exhibits the well known architecture as fibers running mostly left to right communicating between the cerebral hemispheres. Due to the continuous nature of fiber tracking, the corpus callosum also extends laterally to part of the external capsule. Panel e presents fimbria and its connections with hippocampus (yellow) and septal nuclei (brown). The fibers from fimbria begin from the alveus of the left and right hippocampus in a whirling way, meet in the midline under the corpus callosum, and head into the septal nuclei (here starting to be termed as fornix). The fimbria tract (white) also aligns well with the fimbria region (green) identified in the reference brain (WHS).

The printed media clearly limits us in the exploration of this multidimensional data. The diffusion tensor data is so rich that the choice of display method can (and should) be driven by the context of the question. Thus, all the data has been made freely available to the neuroscience community using the database tools developed under the Mouse Bioinformatics Research Network (MBIRN) (Johnson et al., 2007). Interested users can register at <www.civm.duhs.duke.edu/neuro200902/index.html> to download any of the data shown here and MBIRN Atlasing Toolkit (MBAT), a flexible software package for the simultaneous 3D display of multiple datasets (Boline, J. et al, 2007) <cms.loni.ucla.edu/MBAT>.

DISCUSSION

A number of authors have elegantly demonstrated the utility of DTI in understanding the global structure of the mouse brain and the intricate connectivity. For example, the hippocampus of the mouse brain has been delineated in exquisite detail at 80×80×80 μm resolution with a total acquisition time of 17 hours. However, since a bigger FOV is required to image the entire mouse brain, image resolution is limited to 156×156×156 μm with the same size image arrays (Zhang et al., 2002). Other DTI studies of adult mouse brain have been executed at limited resolution due to the constraints of SNR, scan time, and image array size, e.g. 120×120×120 μm resolution with 24-hour scan time (Verma et al., 2005), 133×131×100 μm resolution with 24-hour scan time (Zhang et al., 2005), and 117×117×500 μm resolution with 3.3-hour scan time (Harms et al., 2006). The work shown here has increased the spatial resolution by 20-times over previous work, while still covering the entire adult mouse brain. The scan time is comparable with previous studies, although theoretically, scan time would be 400-times greater to compensate for signal decrease due to the smaller voxels. The higher resolution allows better delineation of anatomy, e.g. the habenular commissure (Fig. 5a) and very thin branches of the optic tract and fimbria (Fig. 5b). Moreover, the higher resolution helps reduce the volume averaging that leads to ambiguity in tractography. The high-quality DTI images shown in Fig. 5 and fiber reconstruction shown in Fig. 6 demonstrate the effectiveness of this DTI protocol, which will become a useful tool to study the mouse brain integrity and white matter architecture at resolution approaching conventional optical histology, while providing quantitative 3D anatomy, diffusion, and directional information that is virtually impossible to gather with conventional histology.

Although not as time-consuming as the histological method, the total acquisition time (28 hours) of this DTI protocol is still long. But the use of active staining, automated scripts for acquiring and processing the data, extended dynamic range acquisition, automated registration, and the rest of the hardware and software infrastructure to facilitate the image pipeline for large arrays now make it feasible to acquire this high-resolution data in a robust and repeatable

fashion. Lower-resolution data at 86 μm isotropic resolution (with voxels about 3-times smaller than the highest-resolution studies published previously (Verma et al., 2005; Zhang et al., 2005) can be acquired in < 3 hours, making survey of interesting models quite tractable. And once appropriate candidate specimens are identified, the automated process can be readily executed with higher resolution. The scan time is no longer the rate-limiting step. The complicated series of computational steps required to reconstruct, register, transform, diagonalize, track, and visualize the data have similarly been streamlined, so the rate-limiting step in the future will be our ability to understand and integrate the data into our collective knowledge base. Work is now under way to facilitate this step.

The DTI data available from the Center for In Vivo Microscopy web site <www.civm.duhs.duke.edu/neuro200902/index.html> has been registered to a common space so that other MR data, conventional histology data, in vivo, and ex vivo data can all be displayed in this common reference frame. Provision of this reference frame is even more important for DTI data than for conventional MR histology data, since the designation of the display coordinate defines both the anatomical landmarks and the eigenvectors direction for the DTI measurements. For example, rotation of the longitudinal axis (from olfactory bulb to cerebellum) would alter both the anatomy viewed in the cardinal plane and the effective color scale indicating fiber orientation, especially the red component assigning to the rostral to caudal direction. Thus, the comparison of DTI data requires considerable attention to the reference coordinate. Moreover, the manually segmented anatomical regions in the WHS space can be applied to define regions in newly acquired brains. (The definition of more regions in the reference brain is in progress.) This standardized coordinate space will facilitate qualitative or quantitative, comparative or collective analysis of the mouse brain. As a future application, the acquisition of more DTI datasets will serve to build a probabilistic atlas of the normal mouse brain, to help characterize normal mouse populations and phenotype mouse disease models.

Acknowledgments

We are grateful to Boma Fubara for assistance in specimen preparation and anatomical region definition, Gary Cofer for assistance in MR acquisition, Jeffrey Brandenburg for assistance in 3D visualization, Alexandra Badea for assistance in anatomical region definition and fiber tracking, and Sally Zimney for assistance in manuscript preparation. All work was performed at the Duke Center for In Vivo Microscopy, an NCRR National Biomedical Technology Research Center (P41 RR005959) and Small Animal Imaging Resource Program (U24 CA092656), with specific support from the Mouse Bioinformatics Research Network (U24 RR021760).

REFERENCES

Alexander DC, Pierpaoli C, Basser PJ, Gee JC. Spatial transformations of diffusion tensor magnetic resonance images. IEEE Transactions on Medical Imaging 2001;20:1131–1139. [PubMed: 11700739]

Badea A, Johnson GA, Williams RW. Genetic dissection of the mouse brain using high-field magnetic resonance microscopy. NeuroImage 2009;45:1067–1079. [PubMed: 19349225]

Badea A, Nicholls PJ, Johnson GA, Wetsel WC. Neuroanatomical phenotypes in the Reeler mouse. NeuroImage 2007;34:1363–1374. [PubMed: 17185001]

Basser PJ, Mattiello J, Lebihan D. MR diffusion tensor spectroscopy and imaging. Biophysical Journal 1994;66:259–267. [PubMed: 8130344]

Boline, J.; Bug, W.; Zaslavsky, I.; Williams, R.; Martone, M.; Anderson, S.; Wong, W.; Yuan, H.; Memon, A.; Ng, Q.; Grethe, J.; Sforza, D.; MacKenzie-Graham, A.; Nissanov, J.; Gustafson, C.; Toga, A. Accessing a sharing infrastructure with the Mouse BIRN atlasing toolkit (MBAT).. Proceedings of the Society for Neuroscience 37th Annual Meeting; San Diego, CA, USA. 2007.

Chesler EJ, Wang JT, Lu L, Qu YH, Manly KF, Williams RW. Genetic correlates of gene expression in recombinant inbred strains - A relational model system to explore neurobehavioral phenotypes. Neuroinformatics 2003;1:343–357. [PubMed: 15043220]

Harms MP, Kotyk JJ, Merchant KM. Evaluation of white matter integrity in ex vivo brains of amyloid plaque-bearing APPsw transgenic mice using magnetic resonance diffusion tensor imaging. Experimental Neurology 2006;199:408–415. [PubMed: 16483571]

Jiang HY, van Zijl PCM, Kim J, Pearlson GD, Mori S. DtiStudio: Resource program for diffusion tensor computation and fiber bundle tracking. Computer Methods and Programs in Biomedicine 2006;81:106–116. [PubMed: 16413083]

Johnson GA, Ali-Sharief A, Badea A, Brandenburg J, Cofer G, Fubara B, Gewalt S, Hedlund LW, Upchurch L. High-throughput morphologic phenotyping of the mouse brain with magnetic resonance histology. NeuroImage 2007;37:82–89. [PubMed: 17574443]

Johnson GA, Cofer GP, Gewalt SL, Hedlund LW. Morphologic phenotyping with MR microscopy: The visible mouse. Radiology 2002;222:789–793. [PubMed: 11867802]

Maudsley AA. Dynamic-range improvement in NMR imaging using phase scrambling. Journal of Magnetic Resonance 1988;76:287–305.

Miller MI, Beg MF, Ceritoglu C, Stark C. Increasing the power of functional maps of the medial temporal lobe by using large deformation diffeomorphic metric mapping. Proceedings of the National Academy of Sciences of the United States of America 2005;102:9685–9690. [PubMed: 15980148]

Mistry NN, Hsu EW. Retrospective distortion correction for 3D MR diffusion tensor microscopy using mutual information and Fourier deformations. Magnetic Resonance in Medicine 2006;56:310–316. [PubMed: 16773654]

Mori S, Crain BJ, Chacko VP, van Zijl PCM. Three-dimensional tracking of axonal projections in the brain by magnetic resonance imaging. Annals of Neurology 1999;45:265–269. [PubMed: 9989633]

Mori S, Itoh R, Zhang JY, Kaufmann WE, van Zijl PCM, Solaiyappan M, Yarowsky P. Diffusion tensor imaging of the developing mouse brain. Magnetic Resonance in Medicine 2001;46:18–23. [PubMed: 11443706]

Paxinos, G.; Franklin, KBJ. The Mouse Brain in Stereotaxic Coordinates. 2nd ed.. Academic Press; New York: 2001.

Pierpaoli C, Basser PJ. Toward a quantitative assessment of diffusion anisotropy. Magnetic Resonance in Medicine 1996;36:893–906. [PubMed: 8946355]

Song SK, Yoshino J, Le TQ, Lin SJ, Sun SW, Cross AH, Armstrong RC. Demyelination increases radial diffusivity in corpus callosum of mouse brain. NeuroImage 2005;26:132–140. [PubMed: 15862213]

Verma R, Mori S, Shen DG, Yarowsky P, Zhang JY, Davatzikos C. Spatiotemporal maturation patterns of murine brain quantified by diffusion tensor MRI and deformation-based morphometry. Proceedings of the National Academy of Sciences of the United States of America 2005;102:6978–6983. [PubMed: 15860588]

Woods RP, Grafton ST, Holmes CJ, Cherry SR, Mazziotta JC. Automated image registration: I. General methods and intrasubject, intramodality validation. Journal of Computer Assisted Tomography 1998;22:139–152. [PubMed: 9448779]

Xu DR, Mori S, Shen DG, van Zijl PCM, Davatzikos C. Spatial normalization of diffusion tensor fields. Magnetic Resonance in Medicine 2003;50:175–182. [PubMed: 12815692]

Xue R, van Zijl PCM, Crain BJ, Solaiyappan M, Mori S. In vivo three-dimensional reconstruction of rat brain axonal projections by diffusion tensor imaging. Magnetic Resonance in Medicine 1999;42:1123–1127. [PubMed: 10571934]

Zhang JY, Miller MI, Plachez C, Richards LJ, Yarowsky P, van Zijl P, Mori S. Mapping postnatal mouse brain development with diffusion tensor microimaging. NeuroImage 2005;26:1042–1051. [PubMed: 15961044]

Zhang JY, van Zijl PCM, Mori S. Three-dimensional diffusion tensor magnetic resonance microimaging of adult mouse brain and hippocampus. NeuroImage 2002;15:892–901. [PubMed: 11906229]

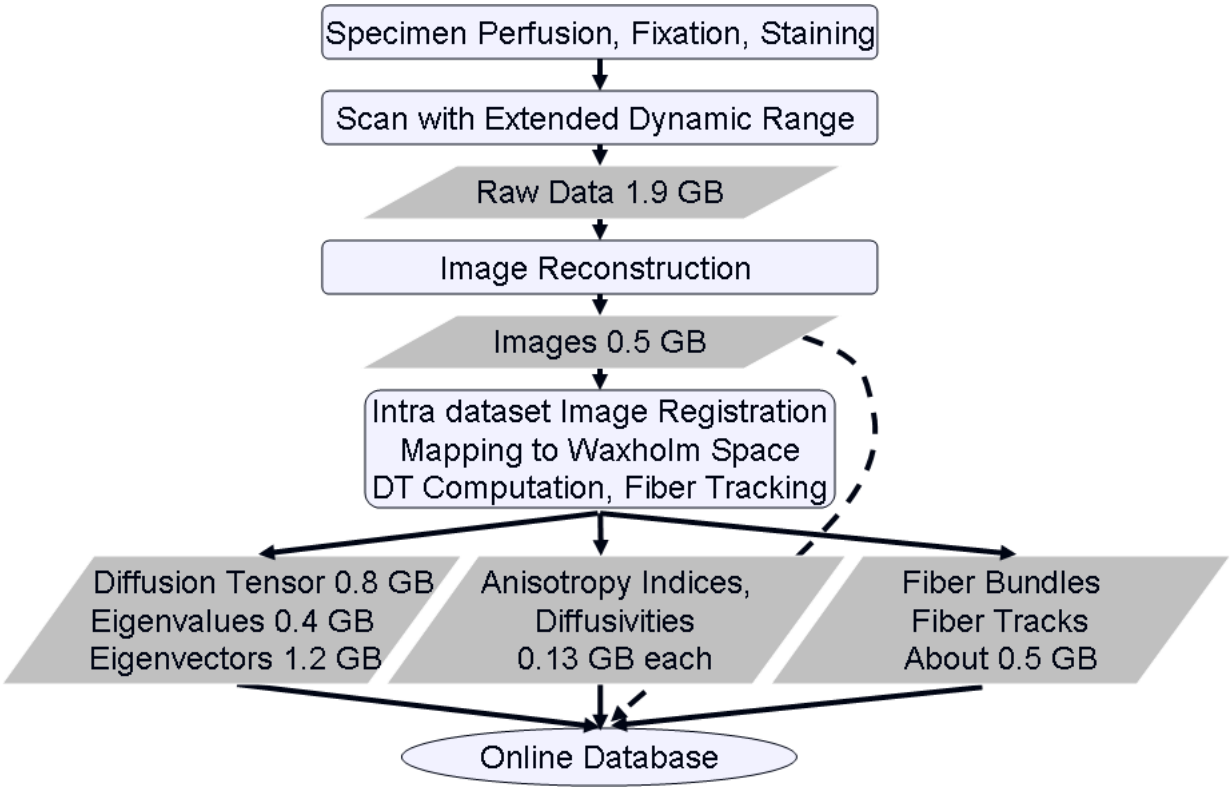

Fig. 1.

The schematic describes the process for high-resolution DTI of the mouse brain. As the brain is fixed and stained, the critical metadata on the animal specimen are entered into the database. A novel acquisition strategy encodes Fourier (k) space while amplifying the high-frequency information. Dedicated computers reconstruct and properly scale the image arrays, as well as automatically archive image data and critical acquisition/reconstruction parameters in the Oracle database. Post-processing steps, including intra-dataset image registration, transformation to the reference space (WHS), diffusion tensor (DT) computation and diagonalization, calculation of other diffusion parameters such as the anisotropy indices, and fiber tracking, provide additional derived data, all of which is assimilated into the database with the animal metadata. The entire database is made available via the BIRN infrastructure providing online access to the original and derived DTI images of the mouse brain.

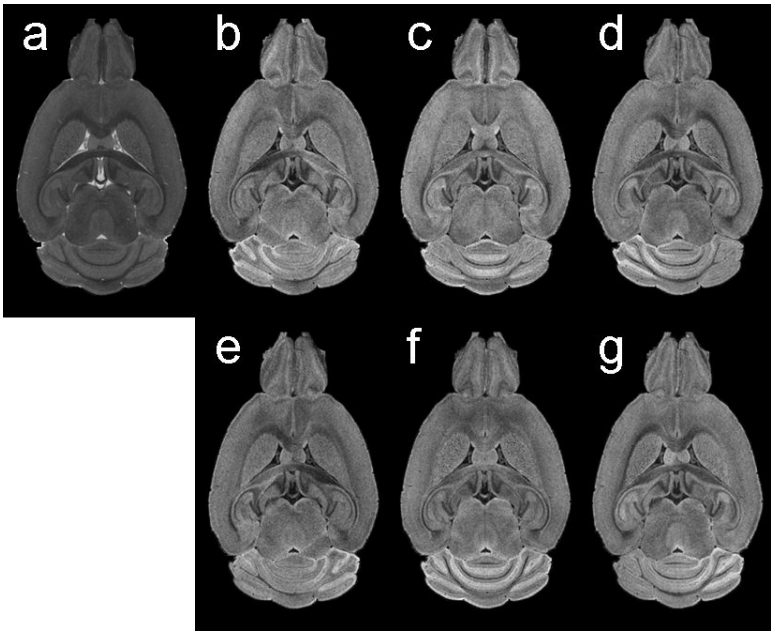

Fig. 2.

Horizontal view of the original b0 (a) and six DWI (b-g) images of an exemplary mouse brain after skull stripping, with diffusion weighting directions of b: [1, 1, 0], c: [1, 0, 1], d: [0, 1, 1], e: [–1, 1, 0], f: [1, 0, –1], and g: [0, –1, 1] at $b \approx 1.5 \times 10^3$ s/mm^2. The intensity of each DWI image was scaled up 3 times.

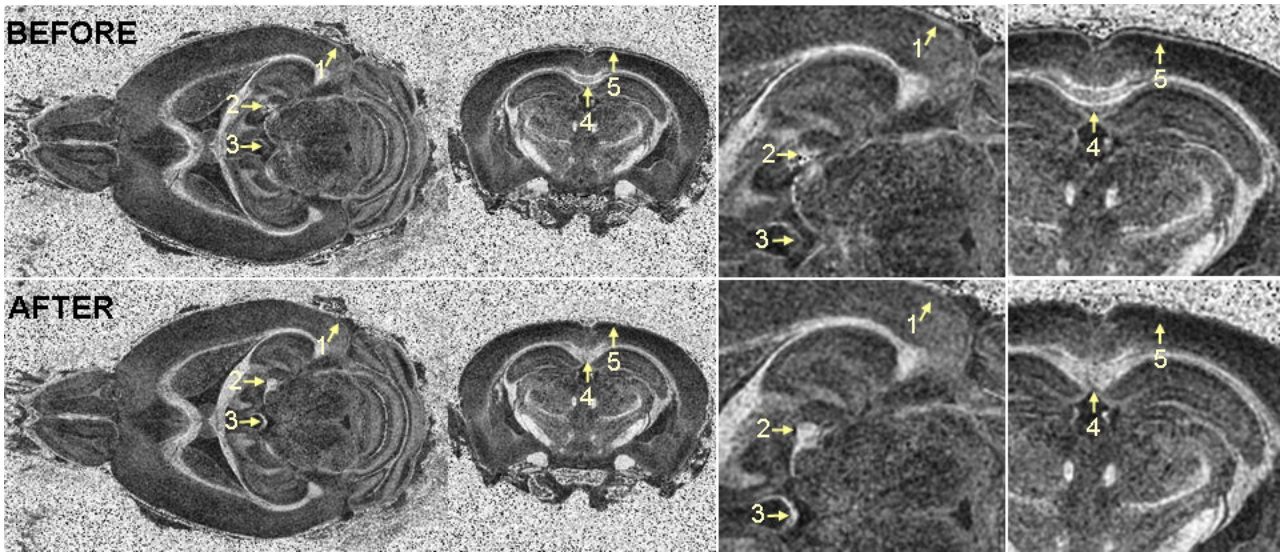

Fig. 3.

Two orthogonal planes of the fractional anisotropy (FA) map of a mouse brain before (top row) and after (bottom row) the intra-dataset registration. Two magnified views are displayed on the right with arrows indicating a few examples of image difference before and after registration.

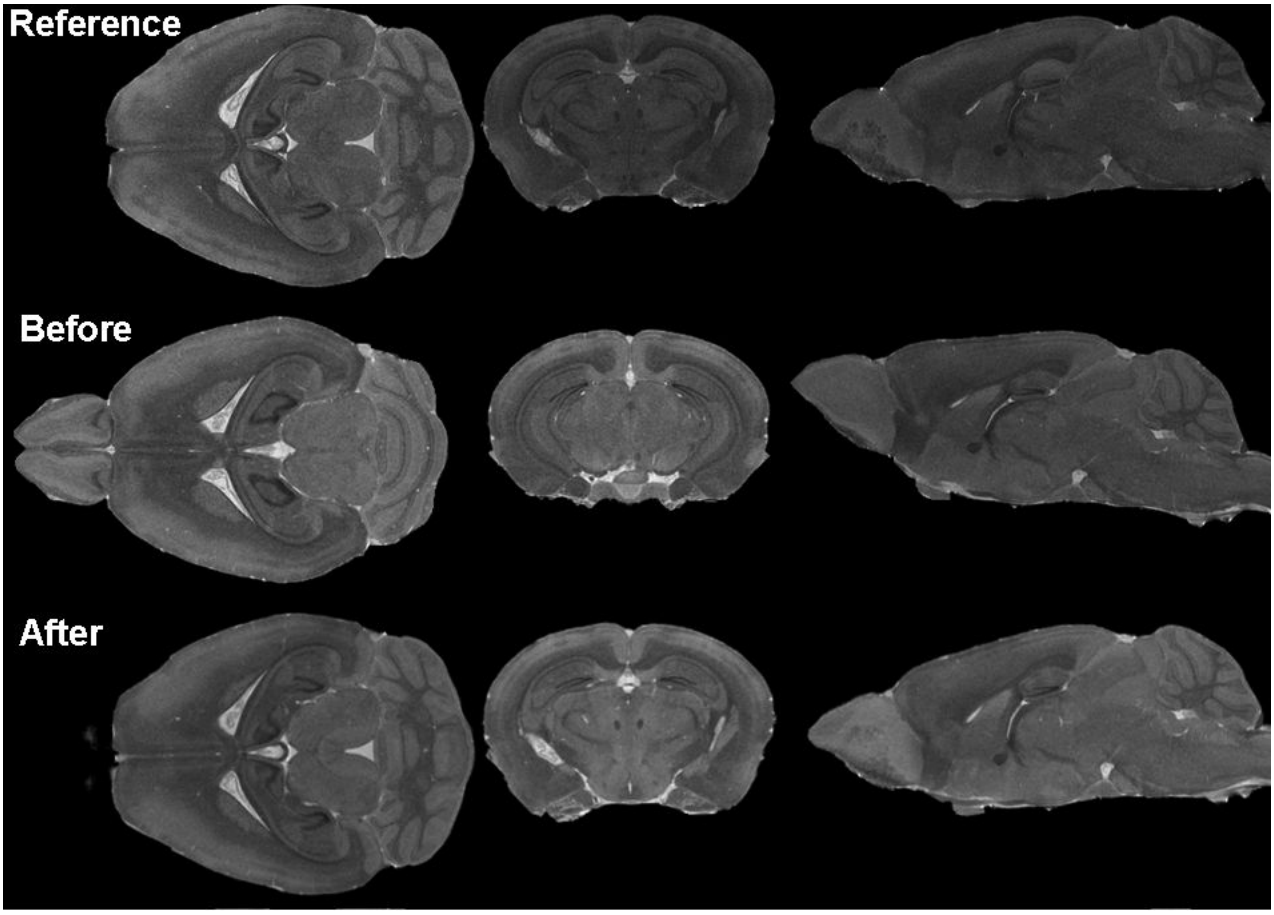

Fig. 4.
T1 images of the reference mouse brain in Waxholm Space (top row), and T1 images of an individual mouse brain in this study before (middle row) and after (bottom row) mapping to the reference brain, showing three orthogonal planes.

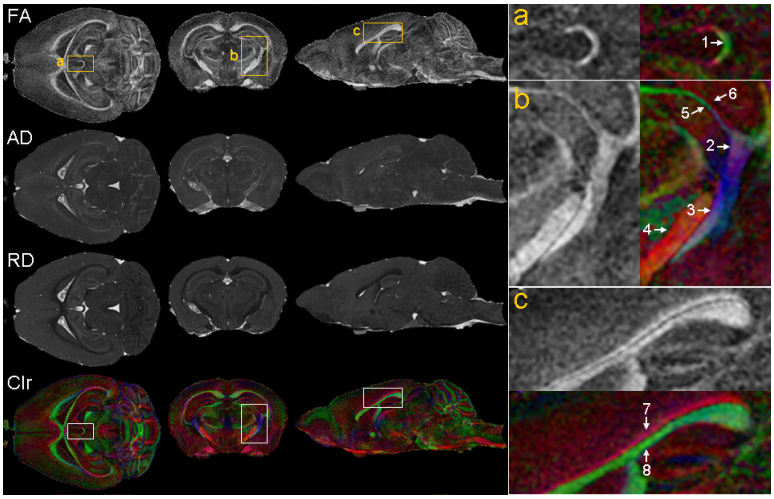

Fig. 5.

FA (fractional anisotropy), AD (axial diffusivity), RD (radial diffusivity), and Clr (color-coded orientation map of the primary eigenvector. Green: left-to-right; Red: rostral-to-caudal; Blue: dorsal-to-ventral) of a mouse brain in three orthogonal planes. The right column shows magnified views that correspond to the regions specified by the rectangles (a, b, and c) in the left column. Arrows indicate some structures that are betterdiscernible with interesting directional information on the colormap.

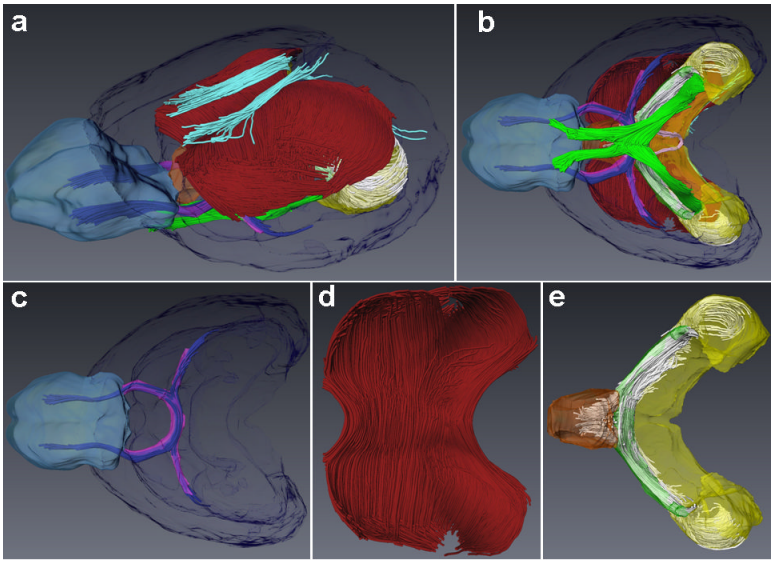

Fig. 6.

A side view (a) and a bottom (ventral) view (b) of the 3D reconstruction of some exemplary fiber tracts obtained from an individual brain overlaid with a few labeled anatomical regions defined in the reference brain (rostral on left and caudal on right). The displayed white matter structures are: corpus callosum (red), cingulum (cyan), anterior commissure (blue), fimbria (white), optic tract (green), and habenular commissure (pink). The displayed anatomical regions in transparent color are: olfactory bulbs (light blue), anterior commissure (purple), fimbria (green), hippocampus (yellow), septal nuclei (brown), and cerebral cortex (dark blue). Several structures are magnified in panels c (anterior commissure), d (corpus callosum), and e (fimbria) showing from the bottom (ventral) view. All labels are defined according to Paxinos (Paxinos and Franklin, 2001).